Pergamon

Atmospheric Environment Vol. 31, No. 2, pp. 131–144, 1997

PII: S1352-2310(96)00202-6
1352-2310/97 $15.00 + 0.00

DEVELOPMENT AND APPLICATION OF A NEW AIR POLLUTION MODELING SYSTEM—II. AEROSOL MODULE STRUCTURE AND DESIGN

MARK Z. JACOBSON

Department of Civil Engineering, Stanford University, Stanford, CA 94305-4020, U.S.A.

(*First received* 5 *March* 1996 *and in final form* 21 *June* 1996)

Abstract—The methods used for simulating aerosol physical and chemical processes in a new air pollution modeling system are discussed and analyzed. Such processes include emissions, nucleation, coagulation, reversible chemistry, condensation, dissolution, evaporation, irreversible chemistry, sedimentation, dry deposition, and radiative scattering and absorption by particles. A new particle size bin structure that nearly eliminates numerical diffusion during growth but still treats nucleation, emissions, coagulation, and transport realistically is discussed. In addition, coagulation is shown to reduce the number and volume concentration of particles less than 0.2 μm in diameter both in the presence and absence of modest rates of particle growth. However, when significant growth occurs, the effect of coagulation is reduced. Further, while sulfate production due to SO_2 dissolution and oxidation in cloud drops is confirmed to be important, it is shown here that such production in aerosols is small over time periods simulated in urban air pollution models. Finally, light scattering and absorption coefficient predictions, obtained by applying a Mie code for stratified spheres, are discussed and shown to match data for a given scenario. Remaining processes in the aerosol module are described. Copyright © 1996 Published by Elsevier Science Ltd

Key word index: Air quality model, size bin structures, coagulation, condensation, chemical equilibrium, aqueous chemistry, aerosol microphysics.

1. INTRODUCTION

The accumulation of aerosols in the Los Angeles Basin and other urban areas is a recognized pollution problem. For example, in 1990, sub-10 μm particulate matter (PM_{10}) concentrations in Los Angeles exceeded the state standard of 30 $\mu g\,m^{-3}$ (annual geometric mean) at all 18 PM_{10} monitoring stations (SCAQMD/SCAG, 1991). To simulate the changes in aerosol size and composition in an urban, regional, or global air pollution model, dynamical, physical, and chemical processes need to be accounted for. These include nucleation, emissions, coagulation, chemical equilibrium, condensation, evaporation, aqueous chemistry, sedimentation, deposition, and transport. Also, gas emissions, gas chemistry, radiative transfer, and meteorology should be predicted.

To date, a handful of models have been used to simulate aerosol processes in urban or free tropospheric regions. For example, Russell and Cass (1986) simulated urban aerosol nitrate production along a Lagrangian trajectory. Similarly, Pilinis *et al.* (1987) simulated the dynamics of multicomponent aerosols along a trajectory in Los Angeles. A trajectory model was also used by Pandis *et al.* (1992, 1993) to study the formation, transport, and deposition of secondary organic aerosols. In addition, Russell *et al.* (1988a, b), Pilinis and Seinfeld (1988), and Bassett *et al.* (1991) simulated aerosols on an Eulerian grid using offline or interpolated meteorology, and Wexler *et al.* (1994) developed equations and techniques to be used in an Eulerian aerosol model. Finally, models used to simulate aerosol processes in the free troposphere include those by Lin *et al.* (1992), Raes *et al.* (1993), Benkovitz *et al.* (1994), Pandis *et al.* (1994), Russell *et al.* (1994), Ackerman *et al.* (1995), and Kasibhatla (1995), among others.

For this study, a new model, GATOR/MMTD, is used. GATOR is a *g*as, *a*erosol, *t*ransport, and *r*adiation Eulerian air quality model (Jacobson, 1994; Jacobson *et al.*, 1996a), and the MMTD is a *m*esoscale *m*eteorological and *t*racer *d*ispersion model (Lu and Turco, 1995; Lu *et al.*, 1996). The coupled model was recently used to study gas-phase pollution buildup in the Los Angeles Basin (Jacobson *et al.*, 1996a). In this work, the aerosol codes in GATOR are described and analyzed. Such codes can be applied, with modification, for urban, regional or global simulations. However, in a follow-up paper, model results are compared to data for an urban case (Jacobson, 1996a).

In the next sections, the aerosol portion of the model is described. In addition, a size bin structure that nearly eliminates numerical diffusion during particle growth but treats nucleation, emissions,

coagulation, and transport effectively, is introduced. Third simulations of coagulation alone, growth coupled to coagulation, and growth alone are compared to each other for an urban case to estimate whether coagulation is important in urban air pollution studies. Irreversible aqueous chemistry is also discussed. Fourth, simulations were performed to determine whether dissolution and oxidation of SO_2 within aerosols are important processes during an urban pollution time scale. Finally, a comparison of scattering and absorption calculations are compared to data for a time and location in the Los Angeles basin.

2. DESCRIPTION OF THE MODEL

2.1. *Overview*

The GATOR/MMTD model solves several equations. Among these are (a) the continuity equations for trace gas number concentration, water vapor, particle number concentration, particle volume concentration, and air; (b) the conservation of energy equation; (c) the horizontal equations of motion; (d) the hydrostatic equation; and (e) the radiative transfer equation. These equations and their solutions are discussed in references for the model previously cited. Briefly, the continuity equations for air and water vapor, the conservation of energy equation, the equations of motion, and the hydrostatic equation are solved with the MMTD. Vertical and horizontal velocities predicted from that model are used to advect gases and aerosol components in GATOR. The horizontal advection scheme used is a Galerkin method with chapeau functions as finite elements (Toon *et al.*, 1988; Pepper *et al.*, 1979). This method is fourth-order accurate in space and second-order accurate in time (Pepper *et al.*, 1979). Gas chemistry is solved with a sparse-matrix Gear-type code (Jacobson, 1995), and radiative transfer is solved with a wavelength-dependent two-stream code (Toon *et al.*, 1989). Aerosol processes are described as follows.

The continuity equation for particles is divided into two sub-equations, one for particle number concentration and the second for particle volume component concentration. If the total volume of a single particle in a given size category i is defined as v_i (units of cm^3 per particle), then the volume of component q within that particle is $v_{i,q}$. Further, volume concentration (e.g. cm^3 of component per cm^3 air) of component q in particles of size i can be defined as $v_{i,q} = n_i v_{i,q}$, where n_i is the number concentration of particles of size i (e.g. no. particles cm^{-3} air). If two out of three of the variables in this relation are determined numerically, the third is found from the relation. Volume concentration and number concentration are the variables determined numerically.

The continuity equation for number concentration of particles of a given size i is written in horizontal spherical coordinates and the sigma-pressure vertical coordinate as

$$\left[\frac{\partial}{\partial t}\left(\frac{\pi_a n_i R_e^2 \cos\varphi}{\rho_a}\right)\right]_\sigma + \left[\frac{\partial}{\partial \lambda_e}\left(\frac{\pi_a u n_i R_e}{\rho_a}\right) + \frac{\partial}{\partial \varphi}\left(\frac{\pi_a v n_i R_e \cos\varphi}{\rho_a}\right)\right]_\sigma + \frac{\partial}{\partial \sigma}\left(\frac{\pi_a \dot{\sigma} n_i R_e^2 \cos\varphi}{\rho_a}\right) = \frac{\pi_a R_e^2 \cos\varphi}{\rho_a}\left[\mathbf{D}_n + R_{emisn} + R_{depn} + R_{sedn} + R_{nucn} + R_{coagn}\right] \quad (1)$$

where

ρ_a = density of air ($g\,cm^{-3}$),
π_a = difference between model surface and model top pressures (e.g. mb),
R_e = radius of earth (cm),
λ_e = longitude (radians),
φ = latitude (radians),
σ = vertical coordinate,
u = west–east scalar velocity ($cm\,s^{-1}$),
v = south–north scalar velocity ($cm\,s^{-1}$),
$\dot{\sigma}$ = vertical scalar velocity ($\partial\sigma\,s^{-1}$),
$\mathbf{D}_n$ = eddy diffusion term for particle number concentration (partic. cm^{-3} air s^{-1}),
R_{emisn} = rate of surface or elevated particle emissions,
R_{depn} = rate of particle dry deposition to the surface from the bottom layer only,
R_{sedn} = rate of sedimentation to the surface or from one altitude down to another,
R_{nucn} = rate of production of new particles due to homogeneous nucleation,
R_{coagn} = rate of change in number concentration due to coagulation.

All rates in equation (1) are in units of (partic. $cm^{-3}\,s^{-1}$). Further, the continuity equation for volume concentration of particle component q in particles of size i is

$$\left[\frac{\partial}{\partial t}\left(\frac{\pi_a v_{i,q} R_e^2 \cos\varphi}{\rho_a}\right)\right]_\sigma + \left[\frac{\partial}{\partial \lambda_e}\left(\frac{\pi_a u v_{i,q} R_e}{\rho_a}\right) + \frac{\partial}{\partial \varphi}\left(\frac{\pi_a v v_{i,q} R_e \cos\varphi}{\rho_a}\right)\right]_\sigma + \frac{\partial}{\partial \sigma}\left(\frac{\pi_a \dot{\sigma} v_{i,q} R_e^2 \cos\varphi}{\rho_a}\right) = \frac{\pi_a R_e^2 \cos\varphi}{\rho_a}\left[\mathbf{D}_v + R_{emisv} + R_{depv} + R_{sedv} + R_{nucv} + R_{coagv} + R_{c/ev} + R_{dp/ev} + R_{ds/ev} + R_{eqv} + R_{aqv}\right] \quad (2)$$

where

$\mathbf{D}_v$ = eddy diffusion term for particle volume concentration ($cm^3\ cm^{-3}\ s^{-1}$),

R_{emisv} = rate of surface or elevated emissions,

R_{depv} = rate of dry deposition to the surface from the bottom layer only,

R_{sedv} = rate of sedimentation to the surface or from one altitude to another,

R_{nucv} = rate of production due to homogeneous or heterogeneous nucleation,

R_{coagv} = rate of change in volume concentration due to coagulation,

$R_{c/ev}$ = rate of production (loss) due to condensational growth (evaporation),

$R_{dp/ev}$ = rate of production (loss) due to depositional growth (evaporation),

$R_{ds/ev}$ = rate of production (loss) due to dissolutional growth (evaporation),

R_{eqv} = rate of change due to reversible chemical equilibrium reactions,

R_{aqv} = rate of change due to irreversible aqueous chemical reactions.

All rates in this equation are in units of (cm^3 partic. cm^{-3} air s^{-1}).

2.2. *Particle size structure*

A historic difficulty in simulating aerosol processes over a three-dimensional grid has been treatment of the particle size bin structure. Several types of structures exist, each with advantages, but each with serious disadvantages as well (Jacobson and Turco, 1995). The most basic size structures are the full-stationary and full-moving size structures.

Briefly, a full-stationary size structure is one in which particles in a given size bin have a fixed volume, and each size bin contains any number of particles, all of which have the same composition and volume as each other particle in the size bin. When particles grow, their volumes do not change; instead, the number of particles in the original size bin decreases, and the number of particles in a larger size bin increases. Similarly, when two particles coagulate, particle numbers in each size bin, not volumes, change.

The advantages of a full-stationary structure are that it permits reasonably realistic treatment of nucleation, emissions, transport, and coagulation because size bin volumes do not change from time to time or location to location. For example, when homogeneous nucleation occurs, new particles enter the smallest size bin, which has a constant volume in time and space. Similarly, when transport occurs, particles of a given volume move and replace particles of the same total volume in adjacent grid cells.

A disadvantage of the stationary size structure is that particle growth leads to numerical diffusion in diameter space in the same way that Eulerian advection leads to numerical diffusion in horizontal space. For example, one type of stationary structure is a quasi-stationary structure. When growth occurs over this

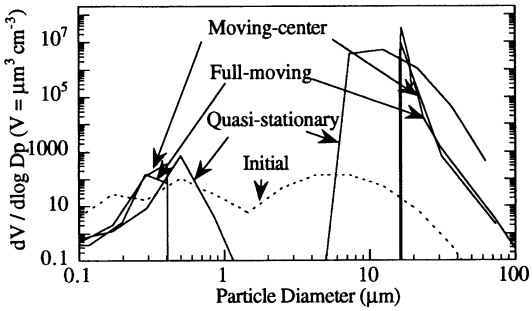

Fig. 1. Comparison of moving-center, full-moving, and quasi-stationary size structure after growth of water onto aerosols to form cloud-sized drops. The initial distribution is shown. Growth occurred when the relative humidity was increased to 100.002% and replenished every 60 s time step for a ten-minute period. Results from the moving-center and full-moving size distribution are non-diffusive and nearly identical. The figure also shows that the quasi-stationary structure is very diffusive.

structure, particles are allowed to grow to their exact sizes, but the new particle volumes are fit back onto a stationary grid in a volume- and number-conserving manner. The fitting method is to split the new volume of particles between two adjacent fixed size bins with the equations, $n_j = n_i(v_k - v_i')/(v_k - v_j)$ and $n_k = n_i(v_i' - v_j)/(v_k - v_j)$. In these equations, v_i' is the average volume of particles in size bin i after growth, n_i is the initial number concentration of particles in the bin, v_j and v_k are the center-volumes of two adjacent fixed size bins ($v_j \leqslant v_i' < v_k$) and n_j and n_k are the additional number concentration of particles added to bins j and k, respectively, due to partitioning. Figure 1 shows that the quasi-stationary structure is numerically diffusive during growth.

A second disadvantage of a stationary structure is that information about the original composition of a particle is lost after growth. For example, when aerosols activate into a fog, core material from many small size bins merge into a few large bins. Thus, upon evaporation, the redistribution of the core material back to smaller-sized particles is arbitrary, unless past information is stored.

Under a full-moving structure, on the other hand, particles in each size bin grow and evaporate to their exact sizes, eliminating numerical diffusion during growth. Upon evaporation, particles shrink to their original size and composition. However, the full-moving size structure has disadvantages that make it impractical for use in a three-dimensional model. For example, since all particle size bins can grow to large volumes, the number of small particle bins may decrease over time. Thus, in some cases, no real size bin will exist to place nucleated or newly emitted material into. A similar problem arises during transport since, in each grid cell, different size bins grow by different amounts. Thus, particles of a given volume and size bin in one grid cell may be averaged with particles of an extremely different volume yet same size bin in an

adjacent cell. Consequently, the benefits of non-diffusive growth are lost due to such extreme averaging.

Here, a structure that not only maintains the advantageous features of the full-stationary structure but also nearly eliminates numerical diffusion during particle growth within a grid cell is introduced. In this structure, size bin edges are fixed; however, the mean diameter of particles within the size bin is allowed to vary. Thus, the structure is called the moving-center size structure.

Because size bin edges are fixed, nucleation, emissions, coagulation, and transport are treated nearly identically to the way they are treated with a full-stationary structure. However, during growth, particles in a size bin are allowed to grow to their exact sizes. If the average diameter of particles in a given bin grows larger than the high-edge diameter of the bin, then *all* particles in the bin are moved to a single size bin bounding the average diameter. Because all particles are moved to the same size bin and not fractionated between or among two or more size bins, numerical diffusion is eliminated during this step. However, particles that are moved to the larger (or smaller) bin are averaged with other particles in that bin, and particles advected to other grid cells are averaged with other particles in the same bin in the adjacent cell. Thus, numerical diffusion can occur upon growth or transport. However, as shown in Fig. 1, diffusion during growth is small.

Size grid edges in the moving-center structure are defined at the beginning of the simulation and remain fixed, while size grid centers vary. For example, the initial volume center of a size bin can be defined with $v_i = v_1 V_{\text{rat}}^{i-1}$, where v_1 is the volume of particles in the smallest size bin, V_{rat} is the volume-ratio of adjacent size bins, and i is the size bin number. V_{rat} can be any number greater than unity. The initial center volume of the size bin can be set equal to the average of the high- and low-edge volumes ($v_{i,\text{hi}}$ and $v_{i,\text{lo}}$, respectively). Thus,

$$v_1 = \tfrac{1}{2}(v_{i,\text{hi}} + v_{i,\text{lo}}). \tag{3}$$

Further, since the volume of the largest particles in the bin cannot exceed the volume of the smallest particles multiplied by V_{rat}, the volumes of the largest particles are calculated as $v_{i,\text{hi}} = V_{\text{rat}} v_{i,\text{lo}}$. Plugging this equation into equation (3) gives $v_{i,\text{lo}} = 2v_i/(1 + V_{\text{rat}})$. Finally, the volume width of a size bin is

$$\mathrm{d}v_i = v_{i,\text{hi}} - v_{i,\text{lo}} = \frac{2v_{i+1}}{1 + V_{\text{rat}}} - \frac{2v_i}{1 + V_{\text{rat}}}$$

$$= \frac{2v_i(V_{\text{rat}} - 1)}{1 + V_{\text{rat}}}. \tag{4}$$

During a simulation with the moving-center structure, $v_{i,\text{hi}}$, $v_{i,\text{lo}}$, and $\mathrm{d}v_i$ remain fixed while v_i is allowed to vary between $v_{i,\text{hi}}$ and $v_{i,\text{lo}}$. When nucleation, and emissions occur with this structure, new particles enter the bin bounding their diameter, and the new and current particles in the bin are averaged by volume. The result is a new average volume of particles in the same bin, which has constant high and low boundary diameters (and volumes). Similarly, when transport occurs, particles in a size bin with fixed boundary diameters move and replace particles in adjacent grid cells with the same boundary diameters. Finally, when two particles coagulate, they form one particle that is partitioned by volume between the current average volume of two adjacent size bins.

A full-moving structure eliminates all numerical diffusion, and, as shown in Fig. 1, the moving-center structure gives results nearly identical to those from the full-moving structure. Also shown in the figure are results from growth over the quasi-stationary structure, which is numerically diffusive. The difference in computer time requirements for each of the three structures is small.

2.3. *Species simulated*

In the aerosol portion of the model liquids, ions, and solids are simulated in each size bin. Table 1 lists all aqueous, ion, and solid species currently accounted for in the model.

2.4. *Nucleation*

The primary substances to nucleate homogeneously in the atmosphere are sulfuric acid and water, together. However, heterogeneous nucleation rates of sulfuric acid–water are several orders of magnitude larger than homogeneous nucleation rates (e.g., Pilinis *et al.*, 1987). Further, in Los Angeles, where significant particle surface area loadings exist, heterogeneous nucleation rates are amplified. Nevertheless, homogeneous nucleation of sulfuric acid–water can be important near locations such as Long Beach, where significant sulfur dioxide emissions occur (e.g. Wexler *et al.*, 1994).

Early aerosol models of the Los Angeles basin used classical nucleation equations to simulate homogeneous nucleation rates. However, this theory does not predict observed nucleation rates in the atmosphere well (e.g. Raes, 1992). Consequently, several recent models have resorted to empirical parameterization rates of sulfuric acid–water homogeneous nucleation (e.g. Raes, 1992; Pandis *et al.*, 1994; Russell *et al.*, 1994; Wexler *et al.*, 1994). For this study, the parameterization of Pandis *et al.* (1994) and Russell *et al.* (1994) was used. While this parameterization was derived for remote marine conditions, it was applied to Los Angeles because no verified nucleation rate parameterization for urban air exists. While the parameterization may cause error in nucleation rate predictions, such errors may be reduced by the fact that aerosol mass loadings in Los Angeles are dominated by emissions and gas-to-particle growth, and coagulation significantly reduces the number concentration of nucleation-sized particles in the basin.

Table 1. List of aqueous, ionic, and solid species in the model

Chemical formula	Chemical name	Chemical formula	Chemical name
Ionic species			
H^+	Hydrogen ion	NO_3^-	Nitrate ion
Na^+	Sodium ion	NO_2^-	Nitrogen dioxide ion
NH_4^+	Ammonium ion	Cl^-	Chloride ion
OH^-	Hydroxy ion	Cl_2^-	Dichloride ion
HO_2^-	Hydroperoxy ion	$ClOH^-$	Chlorine hydroxide radical
O_2^-	Peroxy ion	HCO_3^-	Bicarbonate ion
HSO_4^-	Bisulfate	CO_3^{2-}	Carbonate ion
SO_4^{2-}	Sulfate	CO_3^-	Carbonate radial ion
HSO_3^-	Bisulfite	$HCOO^-$	Formate
SO_3^{2-}	Sulfite	CH_3COO^-	Acetate
SO_4^-	Sulfate radical	Mg^{2+}	Magnesium ion
SO_5^-	Peroxysulfate radical	Ca^{2+}	Calcium ion
HSO_5^-	Peroxymonosulfate	K^+	Potassium ion
$HOCH_2SO_3^-$	Hydromethanesulfonate	Mn(II)	Soluble manganese (II) ion/complexes
$^-OCH_2SO_3^-$	Oxymethanesulfonate ion	Fe(III)	Soluble iron (III) ion/complexes
Aqueous species			
HNO_3(aq)	Nitric acid	HCHO(aq)	Formaldehyde
HO_2NO_2(aq)	Peroxynitric acid	$H_2C(OH)_2$(aq)	Methylene glycol
OH(aq)	Hydroxyl radical	HCOOH(aq)	Formix acid
H_2O_2(aq)	Hydrogen peroxide	CH_3OH(aq)	Methanol
H_2O(aq)	Water vapor	CH_3O_2(aq)	Methylperoxy radical
O_2(aq)	Molecular oxygen	CH_3OOH(aq)	Methyl hydroperoxide
O_3(aq)	Ozone	CH_3COOH(aq)	Acetic acid
SO_2(aq)	Sulfur dioxide	$CH_3C(O)OONO_2$(aq)	Peroxyacyl nitrate
H_2SO_4(aq)	Sulfuric acid	$CH_3C(O)OOH$(aq)	Peroxyacetic acid
NH_3(aq)	Ammonia	CH_3COCHO(aq)	Methyl gloxyal
HCl(aq)	Hydrochloric acid	$CH_3COCH_3O_2$(aq)	Hydrated methylglyoxal
Cl(aq)	Chlorine atom	$NO_2CH_3C_6H_3OH$(aq)	Nitrocresol
CO_2(aq)	carbon dioxide		

Chemical formula	Chemical name	Index of refraction	Density ($g\,cm^{-3}$)
Solids			
Na_2SO_4(s)	Sodium sulfate	1.48 (1)	2.68 (1)
$NaHSO_4$(s)	Sodium bisulfate	1.48 (6)	2.44 (1)
NaCl(s)	Sodium chloride	1.54 (1)	2.17 (1)
$NaNO_3$(s)	Sodium nitrate	1.59 (1)	2.26 (1)
$(NH_4)_2SO_4$(s)	Ammonium sulfate	1.53 (1)	1.77 (1)
NH_4HSO_4(s)	Ammonium bisulfate	1.47 (1)	1.78 (1)
NH_4Cl(s)	Ammonium chloride	1.64 (1)	1.53 (1)
NH_4NO_3(s)	Ammonium nitrate	1.55 (2)	1.73 (1)
$(NH_4)_3H(SO_4)_2$(s)	Tri ammonium bisulfate	1.53 (7)	1.77 (7)
EC(s)	Elemental carbon	1.96–0.65i (3)	1.25 (4)
OC(s)	Organic carbon	1.55 (2)	1.40 (2)
SiO_2(s)	Silicon dioxide	1.49 (1)	2.32 (1)
Al_2O_3(s)	Aluminum oxide	1.76 (1)	3.97 (1)
Fe_2O_3(s)	Iron (III) oxide	3.01 (1)	5.24 (1)
CaO(s)	Calcium oxide	1.84 (1)	3.30 (1)
K_2O(s)	Potassium monoxide	1.50 (5)	2.32 (1)
Mn_2O_7(s)	Manganese heptoxide	1.60 (5)	2.40 (1)
Pb_2O(s)	Lead suboxide	2.01 (1)	8.34 (1)

Species formula	Species name	Index of refraction	Density ($g\,cm^{-3}$)
Other			
Residual	All other species	1.53–0.005i (2)	2.30 (2)

Note: For the solid species, index of refraction and density data are also given.
(1) Lide (1993); (2) Sloane (1984); (3) Bergstrom (1972) wavelength dependent; (4) Horvath (1995) assuming EC(s) is 50% voids; (5) Wexler *et al.* (1992); (6) assume same as for Na_2SO_4(s); (7) assume same as for $(NH_4)_2SO_4$(s).

2.5. *Primary emissions*

A major source of particles in the Los Angeles basin is direct emissions. The gas and aerosol emissions inventories used for Los Angeles air pollution studies are discussed in Jacobson *et al.* (1996a) and Jacobson (1996a), respectively.

2.6. *Coagulation*

Coagulation affects the number and volume concentrations primarily of small particles. Simulating coagulation in a model is important since, if coagulation is neglected, erroneously large number concentrations of aerosols will be carried around in the model. Even if the total mass concentration of aerosol in the model is correct, the mass will be spread among too many particles. Further, coagulation is important for determining (a) the number concentration of particles that surpass the critical radius required for cloud drop nucleation and growth, (b) the size distribution of particles in the absence of high aerosol growth rates, and (c) the evolution of the size distribution of nucleated and newly emitted materials. Further, in fogs and warm clouds, where the number concentration of liquid drops with large cross sections is significant, coagulation (coalescence) is an important process affecting the size distribution. Since coagulation solutions require relatively little computer time relative to other processes, there is no computational reason to neglect such solutions.

Here, coagulation is shown to affect the number and volume concentrations of particles less than 0.2 μm in diameter when growth is non-existent or moderate but to have less effect when growth is significant. The coagulation algorithm used in the model is a semi-implicit scheme that treats particles with any size distribution. The scheme requires no iteration, and its results have been tested against analytical and fully implicit numerical solutions (Jacobson *et al.*, 1994). Here, the coagulation equations for one multicomponent, size-distributed particle type are given in terms of number and volume concentration, respectively. The final number concentration (time t) of particles in size bin k is predicted by

$$n_{k,t} = \frac{n_{k,t-1} + \dfrac{h}{v_k}\sum_{j=1}^{k}\left\{\sum_{i=1}^{k-1} f_{i,j,k} v_i \beta_{i,j} n_{i,t} n_{j,t-1}\right\}}{1 + h\sum_{j=1}^{N_B}(1 - f_{k,j,k})\beta_{k,j,t-1} n_{j,t-1}} \tag{5}$$

where β is the coagulation kernel ($cm^3\,No.^{-1}\,s^{-1}$) (calculated using the total volume of two particles), i and j denote the size bins of the two coagulating particles, k denotes a size bin to which the coagulated pair is being partitioned, $f_{i,j,k}$ is the fraction of the *total* volume of the coagulated pair ($v_i + v_j$) that is partitioned to bin k, h is the time step (s), and $t - 1$ indicates the initial time. The equations for obtaining the fraction $f_{i,j,k}$ was shown in Jacobson *et al.* (1994). The fraction partitions the total volume of a coagulated pair between two size bins, one with total volume smaller than and one with total volume larger than the total volume of the coagulated pair. When the moving-center size structure is used, the fraction, $f_{i,j,k}$, and the coagulation rate, $\beta_{i,j}$, must be recalculated, using current size bin volumes, before each time interval of coagulation.

The right-hand side of equation (5) requires implicit concentration values (time t). These values can be obtained by solving equation (5) in the order $k = 1$ to $k = N_B$. The final volume concentration of each component q in size bin k is

$$v_{q,k,t} = \frac{v_{q,k,t-1} + h\sum_{j=1}^{k}\left(\sum_{i=1}^{k-1} f_{i,j,k}\beta_{i,j} v_{q,i,t} n_{j,t-1}\right)}{1 + h\sum_{j=1}^{N_B}\{(1 - f_{k,j,k})\beta_{k,j,n_{j,t-1}}\}}. \tag{6}$$

The total coagulation kernel used here is the sum of the kernels for Brownian diffusion (Fuchs, 1964), convective Brownian diffusion enhancement (Pruppacher and Klett, 1978), gravitational collection (Pruppacher and Klett, 1978; Ludlum, 1980), turbulent inertial motion (Saffman and Turner, 1956), and turbulent shear (Saffman and Turner, 1956). For small particles, Brownian coagulation is always the dominant process, while for larger particles all other kernels become important. Consequently, inclusion of the remaining kernels in simulating fog microphysical processes is important.

To demonstrate the effect of coagulation on a particle size distribution, simulations of coagulation alone, coagulation coupled to growth, and growth alone were performed over an urban particle size distribution. The initial size distributions for the simulations were divided into four lognormal modes. Two submodes were set in the accumulation mode in each case, with geometric mean diameters near 0.2 μm and 0.5–0.7 μm, respectively (Hering and Friedlander, 1982; John *et al.*, 1989).

Once the particle distributions were created, coagulation calculations were performed for an 8 h period without interruption by other processes. In addition, growth alone and growth coupled to coagulation were simulated. The only growth process considered was condensation of sulfuric acid. Results of the simulations are shown in Figs 2a and b. Figure 2a shows that coagulation alone caused the number concentrations of particles smaller than 0.2 μm in diameter to decrease and those near 0.3 μm in diameter to barely increase. Growth alone, on the other hand, caused the initial size distribution to shift to the right. The shifting of particles to larger diameters caused the volume concentration of these particles to increase as well (Fig. 2b). When coagulation was combined with growth, the number concentration of particles smaller than 0.2 μm decreased, but growth shifted the distribution to the right, causing the number concentration of particles between 0.2 and 0.5 μm to increase. Thus, growth plus coagulation pushed particles to slightly larger sizes than did growth alone or coagulation alone.

Figure 3 shows a comparison of the growth-only and growth/coagulation solutions from Fig. 2a when both the moving-center and full-moving particle size structures were used. Since the full-moving size structure is non-diffusive with respect to growth, the figure

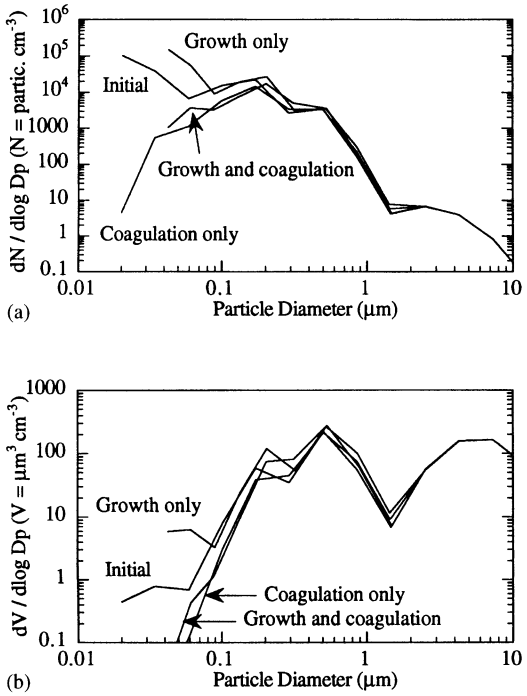

Fig. 2. Estimated change in size-distributed aerosol: (a) number concentration and (b) volume concentration over an 8 h period when coagulation alone, growth alone, and growth coupled to coagulation were considered. Only condensational growth of sulfuric acid was considered. Initial H_2SO_4(g) was 50 $\mu g\,m^{-3}$ and the initial number concentration was 45,070 partic. cm^{-3}. Also, T = 298 K.

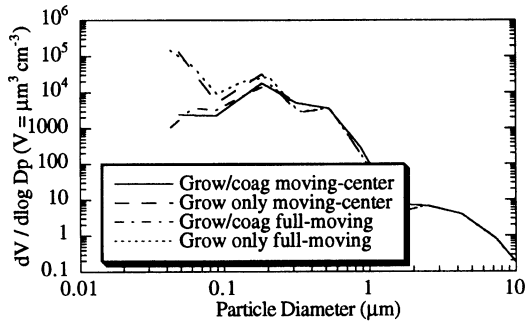

Fig. 3. Comparison of moving-center particle size structure to full-moving size structure for the growth/coagulation and growth-only cases shown in Fig. 2a.

shows that the moving-center size structure is also relatively non-diffusive.

In the second test case of coagulation (Figs 4a and b), both dissolutional and condensational growth were considered. The dissolving species were HNO_3, NH_3, and HCl, and the condensing species was H_2SO_4. Further, in this case, equilibrium equations were solved together with the water equation each time step to estimate liquid water content of particles. When growth occurred, more material converted from the gas to particle phases than in the first test

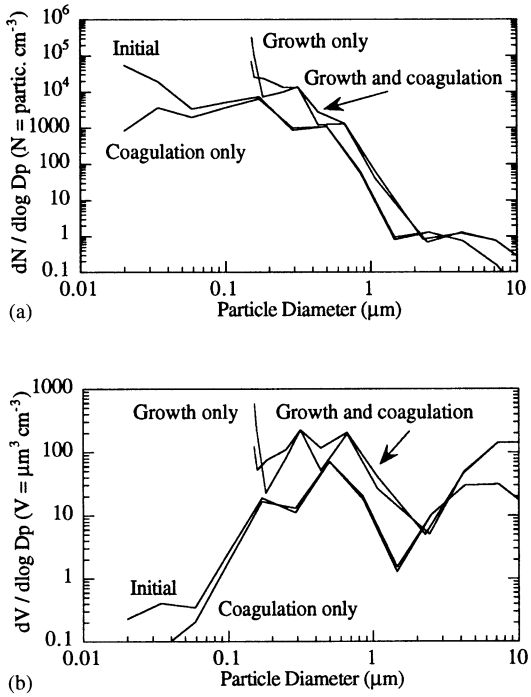

Fig. 4. Estimated change in size-distributed aerosol: (a) number concentration and (b) volume concentration over an 8 h period when coagulation alone, growth alone, and growth coupled to coagulation were considered. Both dissolutional growth of HNO_3, NH_3, and HCl and condensational growth of H_2SO_4 were considered. The particles initially contained sulfate and sodium chloride as well as inert material. When nitric acid and ammonia dissolved, equilibrium equations were solved to determine aqueous partitioning and liquid water content. Sulfuric acid was also allowed to condense from the gas phase. Initial conditions were H_2SO_4 (g) = 15 $\mu g\,m^{-3}$, HNO_3 (g) = 30 $\mu g\,m^{-3}$, NH_3 (g) = 10 $\mu g\,m^{-3}$, HCl (g) = 0 $\mu g\,m^{-3}$, H_2SO_4 (aq) = 10 $\mu g\,m^{-3}$, NaCl (aq) = 15 $\mu g\,m^{-3}$, T = 298 K, and r.h. = 90%.

case. As a result, even the smallest particles in the second case grew to almost 0.2 μm in diameter, and the effects of coagulation on number and volume concentration were less noticeable.

In sum, coagulation affects the number and volume concentration of particles smaller than 0.2 μm in diameter. However, such effects are reduced when growth is coupled to coagulation. Nevertheless, growth plus coagulation pushes particles to slightly larger sizes than does growth alone or coagulation alone.

2.7. *Growth, equilibrium, and aqueous chemistry*

Processes that affect particle volume, but not number, concentration in the model include growth, chemical equilibrium, and aqueous chemistry. Because the rates of equilibrium (reversible) and aqueous (irreversible) reactions are very fast, and because aqueous concentrations affect surface vapor pressures for growth, equilibrium, and aqueous chemistry should be solved nearly simultaneously. Two types of growth processes are considered in the model,

condensation/deposition and dissolution. Species that condense in the model include water at r. h. > 100% and sulfuric acid, among others. The equations for condensational growth/evaporation are

$$\frac{dc_{i,q}}{dt} = k_{i,q}(C_q - B'_{i,q}C_{s,i,q}) + \left(\frac{dc_{i,q}}{dt}\right)_{eq} + \left(\frac{dc_{i,q}}{dt}\right)_{aq} \quad (7)$$

$$\frac{dC_q}{dt} = -\sum_{i=1}^{N_B}\left[k_{i,q}(C_q - B'_{i,q}C_{s,i,q})\right], \quad (8)$$

where $c_{i,q}$ is the mole concentration of species q in size bin i (mol cm^{-3} air), C_q is the ambient vapor concentration of species q in the gas phase (mol cm^{-3} air), $C_{s,i,q}$ is the empirical surface vapor concentration of a condensing species over a flat surface (mol cm^{-3} air), $k_{i,q}$ is the mass transfer rate between the gas phase and all particles of size i (s^{-1}), $B'_{i,q}$ is a Kelvin effect term, $(dc_{i,q}/dt)_{eq}$ is the rapid rate of change in particle concentration of the species due to reversible equilibrium reactions within the particle (e.g. dissociation, precipitation, etc.), and $(dc_{i,q}/dt)_{aq}$ is the rate of change in concentration due to irreversible aqueous chemistry. The mass transfer rate can be estimated as $k_{i,q} = n_i 4\pi r_i D^{eff}_{q,i}$, where $r_{i,t-1}$ is the fluctuating radius of a single particle, and $D^{eff}_{q,i,t-1}$ is an effective diffusion coefficient (cm^2 s^{-1}) that accounts for the geometry of vapor collision with small particles and ventilation of heat and vapor during sedimentation of large particles containing liquid water. A form of the effective diffusion coefficient, as defined here, is given in Jacobson and Turco (1995).

The species that dissolve in the model include, among others, nitric acid, ammonia, hydrochloric acid, sulfur dioxide, and formaldehyde. The equations for dissolutional growth/evaporation are

$$\frac{dc_{i,q}}{dt} = k_{i,q}\left(C_q - B'_{i,q}\frac{c_{i,q}}{H'_{i,q}}\right) + \left(\frac{dc_{i,q}}{dt}\right)_{eq} + \left(\frac{dc_{i,q}}{dt}\right)_{aq} \quad (9)$$

$$\frac{dC_q}{dt} = -\sum_{i=1}^{N_B}\left[k_{i,q}\left(C_q - B'_{i,q}\frac{c_{i,q}}{H'_{i,q}}\right)\right] \quad (10)$$

where $H'_{i,q,t-1}$ is an adjusted Henry's constant (mol aerosol mol^{-1} gas). This term can be written as $H'_{i,q,t-1} = m_q c_{i,w,t-1} R_u T H_q$, where m_q is the molecular weight of the dissolving species, $c_{i,w,t-1}$ is the liquid water content of the aerosol or cloud drop (mol cm^{-3}), R_u is the universal gas constant (kg atm mol^{-1} K^{-1}), T is temperature (K), and H_q is the Henry's constant of the dissolving species (mol kg^{-1} atm^{-1}).

In the model, the growth, equilibrium, and aqueous chemistry terms are time split with a 15 s interval between them. Larger time intervals between growth and equilibrium can cause oscillating predictions of gas and aerosol concentrations (Jacobson, 1996b). The sequence of solution is as follows: (a) intra-aerosol equilibrium is first solved to estimate initial aqueous molalities for the vapor pressure term in equation (9), (b) growth equations are solved between the gas phase and all particle size bins, (c) intra-aerosol equilibrium is solved a second time to partition the mass of material that grew, among liquids, ions, and solids, and (d) aqueous chemistry calculations are performed. This sequence is repeated every 15 s.

Two numerical schemes were developed to solve the $N_B + 1$ growth ordinary differential equations represented by equations (7) and (8), and (9) and (10). These include a sparse-matrix numerical integrator, SMVGEAR II (Jacobson, 1995), and a pair of non-iterative analytical predictor schemes. The growth equations are extremely sparse; thus, the matrices of partial derivatives used in the numerical integrator require no fill-in. The analytical predictor schemes are presented in detail elsewhere (Jacobson, 1996b).

The method used to solve multiple equilibrium, activity coefficient, and water equations together, while conserving mass and charge, is the mass-flux iteration method (Jacobson *et al.*, 1996b). Also, the Zdanovskii–Stokes–Robinson (ZSR) water equation (Stokes and Robinson, 1966) is solved to predict liquid water content due to hydration when the relative humidity is less than 100%.

Finally, irreversible aqueous chemical reactions are similar to gas reactions in that they can be described by first-order, ordinary differential equations (ODEs). SMVGEAR II is used to solve such equations. The chemical reaction mechanism used is shown in Table 2.

Table 2. List of aqueous-phase chemical kinetic reactions, reaction rates, and photoprocesses used in the model

	Reaction	A	B	Ref.
1	$SO_2(aq) + O_3(aq)$–$H_2O(aq) \rightarrow SO_4^{2-} + O_2(aq) + 2H^+$	2.40×10^4		A
2	$HSO_3^- + O_3(aq) \rightarrow SO_4^{2-} + O_2(aq) + H^+$	3.70×10^5	− 18.56	A
3	$SO_3^{2-} + O_3(aq) \rightarrow SO_4^{2-} + O_2(aq)$	1.50×10^9	− 17.72	A
4	$HSO_3^- + H_2O_2(aq) + H^+ \rightarrow SO_4^{2-} + 2H^+ + H_2O(aq)$	7.45×10^7	− 15.96	A
5	SO_3^{2-} + Fe(III)–$O_2(aq)$, $H_2O(aq) \rightarrow SO_4^{2-} + H_2O_2(aq)$ + Fe(III)	9.50×10^7	− 20.27	B,C
6	HSO_3^- + Mn(II)–$O_2(aq)$, $H_2O(aq) \rightarrow SO_4^{2-} + H_2O_2(aq)$ + Mn(II) + H^+	1.00×10^3	− 30.06	Cc,A
7	$HSO_3^- + OH(aq)$–$O_2(aq) \rightarrow SO_5^- + H_2O(aq)$	4.20×10^9	− 5.03	E
8	$SO_3^{2-} + OH(aq)$–$O_2 \rightarrow SO_5^- + OH^-$	4.60×10^9	− 5.03	E
9	$HSO_3^- + CH_3OOH(aq) + H^+ \rightarrow SO_4^{2-} + 2H^+ + CH_3OH(aq)$	1.90×10^7	− 12.75	A
10	$HSO_3^- + CH_3C(O)OOH(aq) \rightarrow SO_4^{2-} + H^+ + CH_3COOH(aq)$	$^x3.60 \times 10^7$ 7.00×10^2	− 13.42	E
11	$HSO_3^- + HO_2(aq) \rightarrow SO_4^{2-} + OH(aq) + H^+$	4.35×10^5		A

Table 2. (*Continued*)

	Reaction	A	B	Ref.
12	$SO_3^{2-} + HO_2(aq) \rightarrow SO_4^{2-} + OH(aq)$	5.65×10^5		A
13	$HSO_3^- + O_2^- \rightarrow SO_4^{2-} + OH(aq)$	4.35×10^4		A
14	$SO_3^{2-} + O_2^- - H_2O(aq) \rightarrow SO_4^{2-} + OH(aq) + OH^-$	5.65×10^4		A
15	$HSO_3^- + HCHO(aq) \rightarrow HOCH_2SO_3^-$	7.90×10^2	-16.44	G
16	$SO_3^{2-} + HCHO(aq) - H_2O(aq) \rightarrow HOCH_2SO_3^- + OH^-$	2.48×10^7	-6.04	G
17	$HOCH_2SO_3^- + OH(aq)\text{–}O_2(aq) \rightarrow SO_5^- + HCHO + H_2O(aq)$	1.40×10^9	-5.03	H
18	$HSO_3^- + Cl_2^- - O_2(aq) \rightarrow SO_5^- + 2Cl^- + H^+$	3.40×10^8	-5.03	D
19	$SO_3^{2-} + Cl_2^-\text{–}O_2(aq) \rightarrow SO_5^- + 2Cl^-$	1.60×10^8	-5.03	D
20	$OH(aq) + HO_2(aq) \rightarrow H_2O(aq) + O_2(aq)$	7.00×10^9	-5.03	I
21	$OH(aq) + O_2^- \rightarrow OH^- + O_2(aq)$	1.00×10^{10}	-5.03	I
22	$OH(aq) + H_2O_2(aq) \rightarrow H_2O(aq) + HO_2(aq)$	2.70×10^7	-5.70	J
23	$2HO_2(aq) \rightarrow H_2O_2(aq) + O_2(aq)$	8.60×10^5	-7.94	K
24	$HO_2(aq) + O_2^- - H_2O(aq) \rightarrow H_2O_2(aq) + O_2(aq) + OH^-$	1.00×10^8	-5.03	K
25	$O_2^- + O_3(aq) - H_2O(aq) \rightarrow OH(aq) + 2O_2(aq) + OH^-$	1.50×10^9	-5.03	I
26	$H_2O_2(aq) + O_3(aq) \rightarrow H_2O(aq) + 2O_2(aq)$	[y] 7.80×10^{-3}		L
27	$HCO_3^- + OH(aq) \rightarrow H_2O(aq) + CO_3^-$	1.50×10^7	-6.41	M
28	$HCO_3^- + O_2^- \rightarrow HO_2^- + CO_3^-$	1.50×10^6		N
29	$CO_3^- + O_2^- - H_2O(aq) \rightarrow HCO_3^- + O_2(aq) + OH^-$	4.00×10^8	-5.03	O
30	$CO_3^- + H_2O_2(aq) \rightarrow HO_2(aq) + HCO_3^-$	8.00×10^5	-9.46	O
31	$O_2^- + Cl_2^- \rightarrow 2Cl^- + O_2(aq)$	1.00×10^9	-5.03	P
32	$H_2O_2(aq) + Cl_2^- \rightarrow 2Cl^- + HO_2(aq) + H^+$	1.40×10^5	-11.31	Q
33	$H_2O_2 + Cl(aq) \rightarrow Cl^- + HO_2(aq) + H^+$	4.50×10^7		R
34	$H_2C(OH)_2(aq) + OH(aq)\text{–}O_2(aq) \rightarrow HCOOH(aq) + HO_2(aq) + H_2O(aq)$	2.00×10^9	-5.03	U
35	$NO_2^- + OH(aq) \rightarrow NO_2(aq) + OH^-$	1.00×10^{10}	-5.03	S
36	$NO_2^- + O_3(aq) \rightarrow NO_3^- + O_2(aq)$	5.00×10^5	-23.32	T
37	$HCOOH(aq) + OH(aq)\text{–}O_2(aq) \rightarrow CO_2(aq) + HO_2(aq) + H_2O(aq)$	1.60×10^8	-5.03	V
38	$HCOO^- + OH(aq)\text{–}O_2(aq) \rightarrow CO_2(aq) + HO_2(aq) + OH^-$	2.50×10^9	-5.03	W
39	$HCOO^- + CO_3^- - H_2O(aq), O_2(aq) \rightarrow CO_2(aq) + HCO_3^- + HO_2(aq) + OH^-$	1.10×10^5	-11.41	X
40	$HCOO^- + C_2^-\text{–}O_2(aq) \rightarrow CO_2(aq) + HO_2(aq) + 2Cl^-$	1.90×10^6	-8.72	Q
41	$CH_3COOH(aq) + OH(aq)\text{–}O_2(aq) \rightarrow HO_2(aq) + CO(aq) + HCHO(aq) + H_2O(aq)$	2.00×10^7	-6.25	Y
42	$CH_3COO^- + OH(aq)\text{–}O_2(l) \rightarrow CO(aq) + HCHO(aq) + H_2O(aq) + O_2^-$	8.00×10^7	-5.07	Y
43	$CH_3C(O)OONO_2(aq) \rightarrow NO_3^- + \text{products}$	4.00×10^{-4}		Z
44	$CH_3O_2(aq) + HO_2(aq) \rightarrow CH_3OOH(aq) + O_2(aq)$	4.30×10^5	-10.07	H
45	$CH_3O_2(aq) + O_2^- - H_2O(aq) \rightarrow CH_3OOH(aq) + O_2(aq) + OH^-$	5.00×10^7	-5.37	H
46	$CH_3OOH(aq) + OH \rightarrow CH_3O_2(aq) + H_2O(aq)$	2.70×10^7	-5.70	H
47	$CH_3OH(aq) + OH(aq)\text{–}O_2(aq) \rightarrow HCHO(aq) + HO_2(aq) + H_2O(aq)$	4.50×10^8	-5.03	W
48	$CH_3OOH(aq) + OH(aq)\text{–}O_2(aq) \rightarrow HCHO(aq) + HO_2(aq) + H_2O(aq)$	1.90×10^7	-6.04	H
49	$SO_5^- + HSO_3^-\text{–}O_2(aq) \rightarrow HSO_5^- + SO_5^-$	3.00×10^5	-10.40	D
50	$SO_5^- + SO_3^{2-} - H^+, O_2(aq) \rightarrow HSO_5^- + SO_5^-$	1.30×10^7	-6.71	D
51	$SO_5^- + O_2^- - H_2O(aq) \rightarrow HSO_5^- + OH^- + O_2(aq)$	1.00×10^8	-5.03	H
52	$SO_5^- + HCOO^-\text{–}O_2(aq) \rightarrow HSO_5^- + CO_2(aq) + O_2^-$	1.40×10^4	-13.42	H
53	$SO_5^- + SO_5^- \rightarrow 2SO_4^- + O_2(aq)$	6.00×10^8	-5.03	D
54	$HSO_5^- + HSO_3^-\text{–}H^+ \rightarrow 2SO_4^{2-} + 2H^+$	7.10×10^6	-10.47	D
55	$HSO_5^- + OH(aq) \rightarrow SO_5^- + H_2O(aq)$	1.70×10^7	-6.38	H
56	$SO_4^- + HSO_3^-\text{–}O_2(aq) \rightarrow SO_4^{2-} + H^+ + SO_5^-$	1.30×10^9	-5.03	H
57	$SO_4^- + HO_2(aq) \rightarrow SO_4^{2-} + H^+ + O_2(aq)$	5.00×10^9	-5.03	H
58	$SO_4^- + O_2^- \rightarrow SO_4^{2-} + O_2(aq)$	5.00×10^9	-5.03	H
59	$SO_4^- + H_2O_2(aq) \rightarrow SO_4^{2-} + H^+ + HO_2(aq)$	1.20×10^7	-6.71	P
60	$SO_4^- + NO_2^- \rightarrow SO_4^{2-} + NO_2(aq)$	9.80×10^8	-5.03	AA
61	$SO_4^- + HCOO^-\text{–}O_2(aq) \rightarrow SO_4^{2-} + CO_2(aq) + HO_2(aq)$	1.10×10^8	-5.03	AA
62	$SO_4^- + Cl^- \rightarrow SO_4^{2-} + Cl(aq)$	2.60×10^8	-5.03	AA
63	$H_2O_2(aq) + h\nu \rightarrow 2OH(aq)$	Radiation dependent		BB
64	$NO_3^- + h\nu - H_2O(aq) \rightarrow NO_2(aq) + OH(aq) + OH^-$	Radiation dependent		BB

Note: For photodissociating species, the reference for the cross-sectional data is listed. The reaction rates (s^{-1}, $M^{-1}\,s^{-1}$, or $M^{-2}\,s^{-1}$) are written in the form

$$K_{aq} = Ae^{B(T_0/T-1)},$$

where A is the reaction rate at 298.16 K, T_0 is the reference temperature (298.16 K), T is temperature (K), and $B = -\Delta H/(R^*T_0)$, where R^* is the ideal gas constant and ΔH is the change in standard enthalpy. x: non-elementary rate expression $K = K_1[H^+] + K_2$, where $K_1 = A_1e^{B(298.15/T-1)}$ and $K_2 = A_2$. y: non-elementary rate expression, $K = K[O_3]^{-0.5}$.

Mechanism derived primarily from Pandis and Seinfeld (1989) and Jacob *et al.* (1989). Individual references: (A) Hoffmann and Calvert (1985); (B) Conklin and Hoffmann (1988); (C) Martin and Hill (1987a); (Cc) Martin and Hill (1987b); (D) Huie and Neta (1987); (E) Lind *et al.* (1987); (G) Boyce and Hoffmann (1984); (H) Jacob (1986); (I) Sehested *et al.* (1968); (J) Christensen *et al.* (1982); (K) Bielski (1978); (aq) Martin (1984); (M) Weeks and Rabani (1966); (N) Schmidt (1972); (O) Behar *et al.* (1970); (P) Ross and Neta (1979); (Q) Hagesawa and Neta (1978); (R) Graedel and Goldberg (1983); (S) Treinin and Hayon (1970); (T) Damschen and Martin (1983); (U) Bothe and Schulte-Frohlinde (1980); (V) Scholes and Willson (1967); (W) Anbar and Neta (1967); (X) Chen *et al.* (1973); (Y) Farhataziz and Ross (1977); (Z) Lee (1984); (AA) Wine *et al.* (1989); (BB) Graedel and Weschler (1981).

Irreversible reactions are solved in the model whenever the liquid water content in an aerosol size bin exceeds 5 $\mu g\,m^{-3}$. Such a threshold could be much higher since it appears that irreversible chemistry is relatively unimportant within aerosols on urban-simulation time scales. For example, Fig. 5 shows a time-dependent comparison of coupled growth, equilibrium, and aqueous chemistry in growing cloud drops when sulfur dioxide dissolution and oxidation are and are not included, respectively, in the calculations. Figure 6 shows the resulting distribution of species in solution after the four-hour simulation. The figures confirm that sulfur dioxide dissolution and oxidation are very important in cloud droplets, even on a short time scale of a few hours.

However, Figs. 7a and b show results after four hours for the no dissolution case and dissolution case, respectively, when aerosols instead of cloud droplets were considered. The conditions for the aerosol simulations were the same as those for cloud drop simulations, except the relative humidity was 90% in the former case but exceeded 100% in the latter case. Figure 7b shows that dissolution and reaction of sulfur dioxide had hardly any effect on the sulfate distribution within aerosols after the 4 h period.

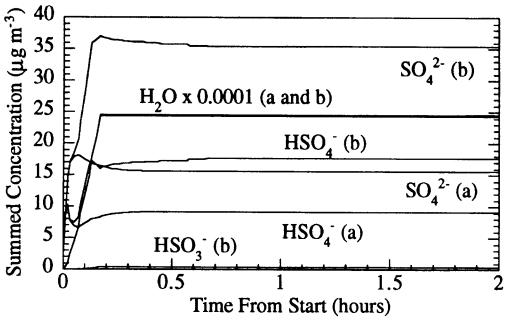

Fig. 5. Time series comparison of sulfate, bisulfate, bisulfite, and water concentrations when cloud drops grew and when sulfur dioxide (a) did not and (b) did dissolve and react in the drops. Initial conditions were $SO_2(g) = 52\ \mu g\,m^{-3}$, $H_2O_2(g) = 10\ \mu g\,m^{-3}$, $HNO_3(g) = 30\ \mu g\,m^{-3}$, $NH_3(g) = 10\ \mu g\,m^{-3}$, $HCl(g) = 0\ \mu g\,m^{-3}$, $H_2SO_4(g) = 15\ \mu g\,m^{-3}$, $H_2SO_4(aq) = 10\ \mu g\,m^{-3}$, NaCl (aq) = 15 $\mu g\,m^{-3}$, $T = 298$ K, r. h. = 100.01% for the first 10 min. Sulfuric acid condensed in both cases.

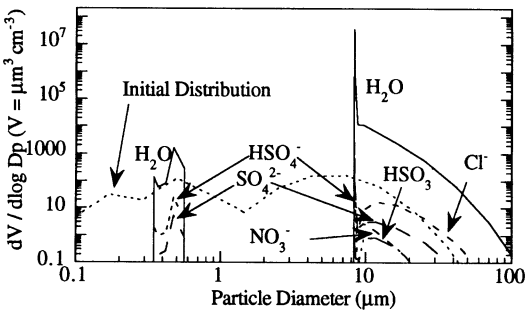

Fig. 6. Initial distribution and final particle composition for the case in Fig. 5 in which sulfur dioxide dissolved and reacted within the cloud drops.

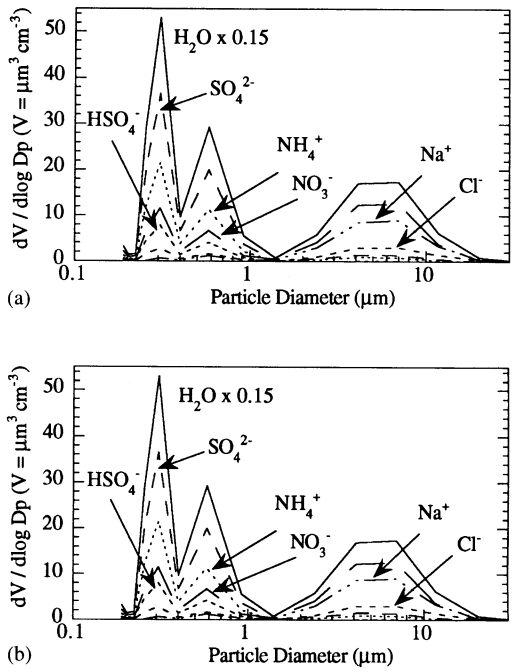

Fig. 7 Particle composition after four hours when sulfur dioxide (a) did not and (b) did grow and react within aerosols. All initial conditions were the same as for Figs 5 and 6 except that the relative humidity here was 90%. The figure shows that sulfur dioxide had little noticeable effect on the sulfate distribution within aerosols after four hours.

2.8. *Sedimentation and dry deposition*

Particle sedimentation is included in model. In sum, size-distributed particles are permitted to fall from one layer of the atmosphere down to any layer below or to the surface. Sedimentation velocities are calculated using a two-step iterative method described in Beard (1976).

Particle dry deposition at the surface in the model is calculated as

$$V_{dp,i} = (R_a + R_b + R_a R_b V_{f,i})^{-1} + V_{f,i} \quad (11)$$

where R_a (aerodynamic resistance) is the resistance to turbulent transfer from the reference height (about 10 m) to the laminar sublayer just above the surface, and R_b (boundary resistance) is the resistance to molecular diffusion through the laminar sublayer (which is about 0.1–0.01 cm deep) (e.g. Seinfeld, 1986). Equations for the aerodynamic and boundary resistances are shown in McRae *et al.* (1982) and Russell *et al.* (1993). Such equations rely on the friction velocity and Monin–Obukhov length, both of which are predicted by the meteorological model.

2.9. *Scattering and absorption*

The model includes calculations of photodissociation rates, radiative heating rates, and meteoro-

logical range. These parameters require spectral extinction coefficient values. Total extinction includes extinction by gas scattering, gas absorption, aerosol scattering, and aerosol absorption. Rayleigh scattering is the only significant gas-scattering light attenuation process. Further, nitrogen dioxide and ozone absorption are the major gas absorption processes. However, nitrogen dioxide affects extinction (and therefore radiative transfer and visibility) only at high mixing ratios and at wavelengths below (about) 500 nm. In the Los Angeles Basin during the 26–29 August 1987 SCAQS period, NO_2 mixing ratios typically ranged from 0.01–0.1 ppmv and occasionally peaked near 0.15 ppmv at some locations during the morning. A typical value was near 0.05 ppmv, which results in an extinction coefficient of about 0.07 km^{-1} at 400 nm and 0.01 km^{-1} at 550 nm. The Koschmieder equation, x (km) $= 3.912/\sigma_{ext}$ ($\lambda = 550$ nm), gives a meteorological range of about 390 km for this latter value. Ozone has a larger effect on extinction than does nitrogen dioxide at wavelengths below about 320 nm. Ozone mixing ratios during SCAQS usually peaked at 0.05–0.25 ppmv. Nevertheless, the cumulative effect of ozone, nitrogen dioxide, and other gases on extinction is relatively small in comparison to the effect of scattering and absorption by particles.

Particle scattering and absorption extinction coefficients in the model are estimated as

$$\sigma_{sp,\lambda} = \sum_{i=1}^{N_B} n_i b_{si,\lambda}, \quad b_{sp,i\lambda} = \pi r_i^2 Q_s(m_\lambda, \alpha_{i,\lambda}) \quad (12)$$

$$\sigma_{ap,\lambda} = \sum_{i=1}^{N_B} n_i b_{ai,\lambda}, \quad b_{ap,i\lambda} = \pi r_i^2 Q_a(m_\lambda, \alpha_{i,\lambda}) \quad (13)$$

respectively. In these equations, n_i is particle number concentration, b is the scattering or absorption cross section of a particle, Q_s is the scattering efficiency, Q_a is the absorption efficiency, m_λ is the complex index of refraction, and $\alpha_{i,\lambda} = 2\pi r_i/\lambda$ is the size parameter. The scattering and absorption efficiencies are determined from a Mie code for stratified spheres (Toon and Ackerman, 1981), using the following setup. First, elemental carbon is assumed to be the core material for Mie calculations. Hematite (α-Fe_2O_3), which is found only near iron ore mining areas, and elemental carbon are primary absorbing particulate species in the atmosphere (Horvath, 1995); however, only elemental carbon is considered here. Second, the real and imaginary indices of refraction of all other components in a particle are volume averaged to obtain an effective complex refractive index for the rest of the particle (e.g. Horvath, 1993). Third, the Mie code is used to calculate spectral scattering, absorption, and backscattering efficiency given the volume of the total particle, the volume of the elemental carbon core, and the associated refractive indices. Default refractive indices for several aerosol species are listed in Table 1. Additionally, wavelength-dependent data for elemental carbon and liquid water were used from Bergstrom (1972) and Hale and Query (1973), respectively.

To demonstrate the optical code, spectral scattering and absorption extinction coefficients were calculated for 4:30 PST on 27 August 1987, at Claremont. The size distribution for this location and time was estimated in the following manner. First, organic carbon, elemental carbon, ammonium, nitrate, sodium, chloride, and total mass concentrations for sub-10 and sub-2.5 μm particles were obtained from SCAQS Sampler data (B. Croes, California Air Resources Board, personal communication). These data were gathered by gravimetric techniques at a relative humidity of about 45% (Countess, 1989). Much of the difference between the total mass and the summed mass of the constituents listed above was due to the presence of additional organic carbon, crustal material, and some liquid water (e.g. Meng *et al.*, 1995). Total organic carbon was crudely estimated by multiplying reported organic carbon mass by 1.4 (Meng *et al.*, 1995). Also, crustal material mass was estimated by first assuming the crustal species were MgO, Al_2O_3, SiO_2, K_2O, CaO, and Fe_2O_3, and then scaling the masses of Mg, Al, etc., observed during SCAQS, to the masses of the respective oxides of these elements (Meng *et al.*, 1995).

Second, the sub-2.5 μm mass of all species, except liquid water, was distributed with three lognormal distributions. The smallest particles were fit into a nucleation mode using lognormal parameters and mass ratios estimated from Whitby (1978). The remaining sub-2.5 μm particles were fit into two accumulation sub-modes. Hering and Friedlander (1982) observed that the mass median diameter of particles containing sulfate was about 0.20 μm on dry days (r. h. 17–68%) and 0.54 μm on moist days (r. h. 26–100%). The lognormal parameters for the sub-modes were estimated from the distribution shown in Eldering *et al.* (1994), which they had fit to data from Claremont for 27 August.

The third step was to distribute particle mass above 2.5 μm with one lognormal mode peaking at about 6.5 μm in diameter. The shape of this mode was roughly fit from the constant value distribution assumed in Eldering *et al.* (1994). A total of 16 size bins were used to represent the distribution. The final step was to estimate liquid water content in each size bin by solving equilibrium equations together with the ZSR water equation. Such calculations were performed at a relative humidity of 45% to be consistent with the fact that gravimetric measurements were taken at approximately this humidity. At 45% humidity, liquid water is a small component of total aerosol mass. Figure 8 shows the number, area, and volume concentration of particles estimated for this time and location.

Mie calculations were performed to determine scattering and absorption efficiencies at each wavelength and particle size given the estimated composition of each particle at each size. Finally, extinction

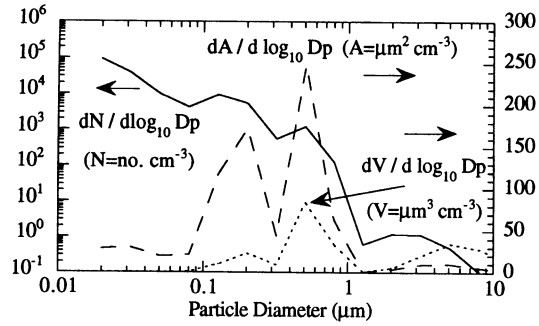

Fig. 8. Number, area, and volume concentration size distribution of the particles that were used in the extinction coefficient calculation for Fig. 9. Sixteen size bins were used to simulate the distribution.

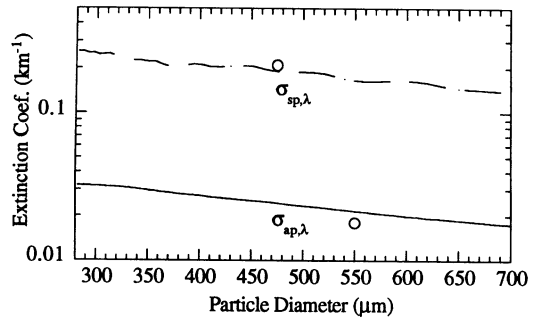

Fig. 9. Aerosol scattering and absorption extinction coefficients calculated using the size distribution in Fig. 8. The circles represent data values.

coefficients at each wavelength were calculated from equations (12) and (13). Results are shown in Fig. 9.

The scattering coefficient measured by General Motors Research Laboratories, (GM) interpolated to 4:30 PST on 27 August, was about 0.21 km^{-1} at 475 nm wavelength (e.g. Eldering *et al.*, 1994). This compares to a predicted value shown in Fig. 9 of 0.19 km^{-1} at 475 nm, for an error of about 9.5%. The measurement was made using a heated inlet nephelometer; thus, the scattering coefficient was obtained for relatively dry particles (Eldering *et al.*, 1994). Since the particle size distribution shown in Fig. 8 was obtained for a relative humidity of 45%, both the size distribution and the scattering measurement were obtained under similar water-content conditions. Finally, at 550 nm, the modeled absorption coefficient was 0.0216 km^{-1}, which compares to a SCAQS Sampler data value of about 0.018 km^{-1}. The resulting error was 20%.

3. CONCLUSION

This paper described the numerical methods used for simulating aerosol processes in the GATOR/MMTD air pollution model. Such processes included coagulation, chemical equilibrium, condensation, dissolution, evaporation, aqueous chemistry, sedimentation, dry deposition, and radiative effects.

Among the new techniques shown here was a size bin structure that nearly eliminates numerical diffusion during particle growth but allows treatment of nucleation, emissions, coagulation, and transport in a manner nearly identical to that treated by a stationary size structure. The structure is simple to implement. In addition, coagulation equations, adapted to the new size bin structure, were shown. Simulations of coagulation alone, growth coupled to coagulation, and growth alone were compared for an urban air pollution case. The simulations showed that coagulation reduced the number and volume concentration of particles less than 0.2 μm in diameter both in the presence and absence of modest rates of particle growth. On the other hand, when growth rates were fast, the effect of coagulation was reduced. Nevertheless, growth plus coagulation pushed particles to slightly larger sizes than did growth alone or coagulation alone. Dissolution and aqueous oxidation were also discussed. Simulations were performed that confirm SO_2 dissolution and oxidation in cloud drops is important over urban simulation time periods; however, such dissolution and oxidation in aerosols is not. Finally, treatment of radiative processes was discussed. Predictions of scattering and absorption coefficients compared well to data for a time and location in the Los Angeles basin.

Acknowledgements—A portion of this work was performed on a Cray J-916, provided in part by Cray Research, Inc. Cray 90 computer support was also given by the San Diego Supercomputer Center, the EPA Supercomputer Center at Bay City, Michigan, and the NAS computer facilities in Mountain View, California. This work was also supported, in part, by grants from the Environmental Protection Agency under assistance agreements 823755-01-0 and 823186-01-0, the Charles Lee Powell Foundation, and the National Science Foundation under agreement ATM-9504481. Although the research described in this article has been funded in part by the United States Environmental Protection Agency, it has not been subjected to the Agency's peer and administrative review and therefore may not necessarily reflect the views of the Agency and no official endorsement should be inferred.

REFERENCES

Ackerman A. S., Toon O. B. and Hobbs P. V. (1995) A model for particle microphysics, turbulent mixing, and radiative transfer in the stratocumulus-topped marine boundary layer and comparisons with measurements. *J. atmos. Sci.* **52,** 1204–1236.

Anbar M. and Neta P. (1967) A compilation of specific bimolecular rate constants for the reactions of hydrated electrons, hydrogen atoms, and hydroxyl radicals with inorganic and organic compounds in aqueous solution. *Int. J. Appl. Radiat. Isot.* **18,** 493–523.

Bassett M. E., Cassmassi J. C., Durkee K. R. and Hogo H. (1991) Episodic PM_{10} model development and application for the South Coast Air Basin. Final Technical Report V–E, South Coast Air Quality Management District.

Beard K. V. (1976) Terminal velocity and shape of cloud and precipitation drops aloft. *J. atmos. Sci.* **33,** 851–864.

Behar D., Czapski G. and Duchovny I. (1970) Carbonate radical in flash photolysis and pulse radiolysis of aqueous carbonate solutions. *J. phys. Chem.* **74,** 2206–2210.

Benkovitz C. M., Berkowitz C. M., Easter R. C., Nemesure S., Wagener R. and Schwartz S. E. (1994) Sulfate over the North Atlantic and adjacent continental regions: evaluation for October and November, 1986 using a three-dimensional model driven by observation-derived meteorology. *J. geophys. Res.* **99,** 20,725–20,756.

Bergstrom R. W. Jr. (1972) Predictions of the spectral absorption and extinction coefficients of an urban air pollution aerosol model. *Atmospheric Environment* **6,** 247–258.

Bielski B. H. J. (1978) Reevaluation of the spectral and kinetic properties of HO_2 and O_2-free radicals. *Photochem. Photobiol.* **28,** 645–649.

Bothe E. and Schulte-Frohlinde D. (1980) Reaction of dihydroxymethyl radical with molecular oxygen in aqueous solution. *Z. Naturforsch. B, Anorg. Chem. Org. Chem.* **35,** 1035–1039.

Boyce S. D. and Hoffmann M. R. (1984) Kinetics and mechanism of the formation of hydroxymethanesulfonic acid at low pH. *J. phys. Chem.* **88,** 4740–4746.

Chen S., Cope V. W. and Hoffman M. Z. (1973) Behavior of CO_3^- radicals generated in the flash photolysis of carbonatoamines complexes of cobalt(III) in aqueous solution. *J. phys. Chem.* **77,** 1111–1116.

Christensen H., Sehested K. and Corfitzen H. (1982) Reactions of hydroxyl radicals with hydrogen peroxide at ambient and elevated temperatures. *J. phys. Chem.* **86,** 1588–1590.

Conklin M. H. and Hoffmann M. R. (1988) Metal ion–S(IV) chemistry III. Thermodynamics and kinetics of transient iron(III)–sulfur(IV) complexes. *Envir. Sci. Technol.* **22,** 891–898.

Countess R. J. (1989) Southern California Air Quality Study Sampler Chemistry, Final Report. Prepared for the California Air Resources Board, Sacramento, California.

Damschen D. E. and Martin L. R. (1983) Aqueous aerosol oxidation of nitrous acid by O_2, O_3, and H_2O_2. *Atmospheric Environment* **17,** 2005–2011.

Eldering A., Cass G. and Moon K. C. (1994) An air monitoring network using continuous particle size distribution monitors: connecting pollutant properties to visibility via Mie scattering calculations. *Atmospheric Environment* **28,** 2733–2749.

Farhataziz and Ross A. B. (1977) Selected specific rates of transients from water in aqueous solutions, III. Hydroxyl radical and perhydroxyl radical and their radical ions. Rep. NSRDBS-NBS 59, U.S. Dept. of Commerce, Washington, District of Columbia.

Fuchs N. A. (1964) *The Mechanics of Aerosols* (translated by Daisley R. E. and Fuchs M.). Pergamon Press, New York.

Graedel T. E. and Goldberg K. I. (1983) Kinetic studies of raindrop chemistry, 1, Inorganic and organic processes. *J. geophys. Res.* **88,** 10,865–10,882.

Graedel T. E. and Weschler C. J. (1981) Chemistry within aqueous atmospheric aerosols and raindrops. *Rev. Geophys.* **19,** 505–539.

Hagesawa K. and Neta P. (1978) Rate constants and mechanisms of reaction for Cl_2^- radicals. *J. phys. Chem.* **82,** 854–857.

Hale G. M. and Querry M. R. (1973) Optical constants of water in the 200-nm to 200-μm wavelength region. *Appl. Opt.* **12,** 555–563.

Hering S. V. and Friedlander S. K. (1982) Origins of aerosol sulfur size distributions in the Los Angeles Basin. *Atmospheric Environment* **16,** 2647–2656.

Hoffmann M. R. and Calvert J. G. (1985) Chemical transformation modules for Eulerian acid deposition models, Vol. 2, the aqueous-phase chemistry. EPA/600/3-85/017, U.S. Environ. Prot. Agency, Research Triangle Park, North Carolina.

Horvath H. (1993) Atmospheric light absorption—a review. *Atmospheric Environment* **27A,** 293–317.

Horvath H. (1995) Size segregated light absorption coefficient of the atmospheric aerosol. *Atmospheric Environment* **29A,** 875–883.

Huie R. E. and Neta P. (1987) Rate constants for some oxidations of S(IV) by radicals in aqueous solutions. *Atmospheric Environment* **21,** 1743–1747.

Jacob D. J. (1986) Chemistry of OH in remote clouds and its role in the production of formic acid and peroxymonosulfonate. *J. geophys. Res.* **91,** 9807–9826.

Jacob D. J., Gottlieb E. W. and Prather M. J. (1989) Chemistry of a polluted cloudy boundary layer. *J. geophys. Res.* **94,** 12,975–13,002.

Jacobson M. Z. (1994) Developing, coupling, and applying a gas, aerosol, transport, and radiation model to study urban and regional air pollution. Ph. D. thesis, Department of Atmospheric Sciences, University of California, Los Angeles.

Jacobson M. Z., Turco R. P., Jensen E. J. and Toon O. B. (1994) Modeling coagulation among particles of different composition and size. *Atmospheric Environment* **28A,** 1327–1338.

Jacobson M. Z. (1995) Computation of global photochemistry with SMVGEAR II. *Atmospheric Environment* **29A,** 2541–2546.

Jacobson M. Z. and Turco R. P. (1995) Simulating condensational growth, evaporation, and coagulation of aerosols using a combined moving and stationary size grid. *Aerosol Sci. Technol.* **22,** 73–92.

Jacobson M. Z., Lu R., Turco R. P. and Toon O. B. (1996a) Development and application of a new air pollution modeling system. Part I: gas-phase simulations. *Atmospheric Environment* **30B,** 1939–1963.

Jacobson M. Z., Tabazadeh A. and Turco R. P. (1996b) Simulating equilibrium within aerosols and non-equilibrium between gases and aerosols. *J. geophys. Res.* **101,** 9079–9091.

Jacobson M. Z. (1996a) Development and application of a new air pollution modeling system. Part III: aerosol-phase simulations. *Atmospheric Environment* (In press).

Jacobson M. Z. (1996b) Numerical techniques to solve condensational and dissolutional growth equations when growth is coupled to reversible reactions. *Aerosol. Sci. Technol.* (In review).

John W., Wall S. M., Ondo J. L. and Winklmayr W. (1989) Final Report for the California Air Resources Board under Contract No. A6-112-32.

Kasibhatla P. S. (1995) Sulfur cycling and aerosol dynamics in the marine boundary layer. *EOS Supplement*, p. F112, American Geophysical Union.

Lee Y.-N. (1984) Atmospheric aqueous-phase reactions of nitrogen species, gas-liquid chemistry of natural waters, Vol. 1, BNL 51757, pp. 20/1–20/10. Brookhaven National Laboratory.

Lide D. R. (ed.-in-chief) (1993) *CRC Handbook of Chemistry and Physics.* CRC Press, Boca Raton, Florida.

Lin X., Chameides W. L., Kiang C. S., Stelson A. W. and Berresheim H. (1992) A model study of the formation of cloud condensation nuclei in remote marine areas. *J. geophys. Res.* **97,** 18,161–18,171.

Lind J. A., Kok G. L. and Lazrus A. L. (1987) Aqueous phase oxidation of sulfur(IV) by hydrogen peroxide, methylhydroperoxide, and peroxyacetic acid. *J. geophys. Res.* **92,** 4171–4177.

Lu R. and Turco R. P. (1995) Air pollutant transport in a coastal environment Part II: three dimensional simulations over the Los Angeles Basin. *Atmospheric Environment* **29B,** 1499–1518.

Lu R., Turco R. P. and Jacobson M. Z. (1996) An integrated air pollution modeling system for urban and regional scales part I: structure and performance. *J. geophys. Res.* (in press).

Ludlum F. H. (1980) *Clouds and Storms.* Pennsylvania State University Press, University Park.

Martin L. R. (1984) Kinetic studies of sulfite oxidation in aqueous solution. In SO_2, NO, *and* NO_2 *Oxidation Mechanisms: Atmospheric Considerations* (edited by Calvert J. G.), pp. 63–100. Butterworth, Stoneham, Massachusetts.

Martin L. R. and Hill M. W. (1987a) The iron-catalyzed oxidation of sulfur: reconciliation of the literature rates. *Atmospheric Environment* **21,** 1487–1490.

Martin L. R. and Hill M. W. (1987b) The effect of ionic strength on the manganese catalyzed oxidation of sulfur(IV). *Atmospheric Environment* **21,** 2267–2270.

McRae G. J., Goodin W. R. and Seinfeld J. H. (1982) Development of a second-generation mathematical model for urban air pollution—I. Model formulation. *Atmospheric Environment* **16,** 679–696.

Meng Z., Seinfeld J. H., Saxena P. and Kim Y. P. (1995) Contribution of water to particulate mass in the South Coast Air Basin. *Aerosol. Sci. Technol.* **22,** 111–123.

Pandis S. N. and Seinfeld J. H. (1989) Sensitivity analysis of a chemical mechanism for aqueous-phase atmospheric chemistry. *J. geophys. Res.* **94,** 1105–1126.

Pandis S. N., Harley R. A., Cass G. R. and Seinfeld J. H. (1992) Secondary organic aerosol formation and transport. *Atmospheric Environment* **26A,** 2269–2282.

Pandis S. N., Wexler A. S. and Seinfeld J. H. (1993) Secondary organic aerosol formation and transport—II. Predicting the ambient secondary organic aerosol size distribution. *Atmospheric Environment* **27A,** 2403–2416.

Pandis S. N., Russell L. M. and Seinfeld J. H. (1994) The relationship between DMS flux and CCN concentration in remote marine regions. *J. geophys. Res.* **99,** 16,945–16,957.

Pepper D. W., Kern C. D. and Long P. E. Jr. (1979) Modeling the dispersion of atmospheric pollution using cubic splines and chapeau functions. *Atmospheric Environment* **13,** 223–237.

Pilinis C., Seinfeld J. H. and Seigneur C. (1987) Mathematical modeling of the dynamics of multicomponent atmospheric aerosols. *Atmospheric Environment* **21,** 943–955.

Pilinis C. and Seinfeld J. H. (1988) Development and evaluation of an eulerian photochemical gas-aerosol model. *Atmospheric Environment* **22,** 1985–2001.

Pruppacher H. R. and Klett J. D. (1978) *Microphysics of Clouds and Precipitation.* Reidel, Hingham, Massachusetts.

Raes F., Van Dingenen R., Wilson J. and Saltelli A. (1993) Cloud condensation nuclei from dimethylsulfide in the natural marine boundary layer: remote vs. in-situ production. In *Dimethylsulfide, Ocean, Atmosphere and Climate* (edited by Restelli G. and Angeletti G.), pp. 311–322. Kluwer, Dordrecht.

Raes F., Saltelli A. and Van Dingenen R. (1992) Modelling formation and growth of H_2SO_4–H_2O aerosols: uncertainty analysis and experimental evaluation. *J. aerosol Sci.* **23,** 759–771.

Ross A. B. and Neta P. (1979) Rate constants for reactions of inorganic radicals in aqueous solutions. NSRDS-NBS 65. National Bureau of Standards, U.S. Department of Commerce, Washington, District of Columbia.

Russell A. G. and Cass G. (1986) Verification of a mathematical model for aerosol nitrate and nitric acid formation and its use for control measure evaluation. *Atmospheric Environment* **20,** 2011–2025.

Russell A. G., McCue K. F. and Cass G. R. (1988a) Mathematical modeling of the formation of nitrogen-containing air pollutants. 1. Evaluation of an Eulerian photochemical model. *Envir. Sci. Technol.* **22,** 263–271.

Russell A. G., McCue K. F. and Cass G. R. (1988b) Mathematical modeling of the formation of nitrogen-containing air pollutants. 2. Evaluation of the effect of emission controls. *Envir. Sci. Technol.* **22,** 1336–1347.

Russell A. G., Winner D. A., Harley R. A., McCue K. F. and Cass G. R. (1993) Mathematical modeling and control of the dry deposition flux of nitrogen-containing air pollutants. *Envir. Sci. Technol.* **27,** 2772–2782.

Russell L. M., Pandis S. N. and Seinfeld J. H. (1994) Aerosol production and growth in the marine boundary layer. *J. geophys. Res.* **99,** 20,989–21,003.

Saffman P. G. and Turner J. S. (1956) On the collision of drops in turbulent clouds. *J. Fluid Mech.* **1,** 16–30.

SCAQMD/SCAG (South Coast Air Quality Management District and Southern California Association of Governments) (1991) 1991 *Air Quality Management Plan: South Coast Air Basin.*

Schmidt K. H. (1972) Electrical conductivity techniques for studying the kinetics of radiation-induced chemical reactions in aqueous solutions. *Int. J. Radiat. Phys. Chem.* **4,** 439–468.

Scholes G. and Willson R. L. (1967) γ-radiolysis of aqueous thymine solutions. Determination of relative reaction rates of OH radicals. *Trans. Faraday Soc.* **63,** 2982–2993.

Sehested K., Rasmussen O. L. and Fricke H. (1968) Rate constants of OH with HO_2, O_2^-, and $H_2O_2^+$ from hydrogen peroxide formation in pulse-irradiated oxygenated water. *J. phys. Chem.* **72,** 626–631.

Seinfeld J. H. (1986) *Atmospheric Chemistry and Physics of Air Pollution.* Wiley, New York.

Sloane C. S. (1984) Optical properties of aerosols of mixed composition. *Atmospheric Environment* **18,** 871–878.

Stokes R. H. and Robinson R. A. (1966) Interactions in aqueous nonelectrolyte solutions. I. Solute–solvent equilibria. *J. phys. Chem.* **70,** 2126–2130.

Toon O. B. and Ackerman T. P. (1981) Algorithms for the calculation of scattering by stratified spheres. *Appl. Opt.* **20,** 3657–3660.

Toon O. B., Turco R. P., Westphal D., Malone R. and Liu M. S. (1988) A multidimensional model for aerosols: description of computational analogs. *J. atmos. Sci.* **45,** 2123–2143.

Treinin A. and Hayon E. (1970) Absorption spectra and reaction kinetics of NO_2, N_2O_3, and N_2O_4 in aqueous solutions. *J. Am. Chem. Soc.* **92,** 5821–5828.

Weeks J. L. and Rabani J. (1966) The pulse radiolysis of dearated aqueous carbonate solutions. *J. phys. Chem.* **70,** 2100–2106.

Wexler A. S., Eldering A., Pandis S. N., Cass G. R., Seinfeld J. H., Moon K. C. and Hering S. (1992) Modeling aerosol processes and visibility based on the SCAQS data. Final report to the California Air Resources Board under contract no. A932-054.

Wexler A. S., Lurmann F. W. and Seinfeld J. H. (1994) Modeling urban and regional aerosols—I. Model development. *Atmospheric Environment* **28A,** 531–546.

Whitby K. T. (1978) The physical characteristics of sulfur aerosols. *Atmospheric Environment* **12,** 135–159.

Wine P. H., Tang Y., Thorn R. P., Wells J. R. and Davis D. D. (1989) Kinetics of aqueous-phase reactions of the SO_4^- radical with potential importance in cloud chemistry. *J. geophys. Res.* **94,** 1085–1094.